



New Principle of Busbar Protection Based on Active Power and Extreme Learning Machine

Syed Hassan Lal Gilani, Xingxing Dong*, Haiyan Xu

School of Automation & Information Engineering, Sichuan University of Science & Engineering, Zigong, China

Email: *domewatson@126.com

How to cite this paper: Gilani, S.H.L., Dong, X.X. and Xu, H.Y. (2020) New Principle of Busbar Protection Based on Active Power and Extreme Learning Machine. *Open Access Library Journal*, 7: e6167. <https://doi.org/10.4236/oalib.1106167>

Received: February 14, 2020

Accepted: May 23, 2020

Published: May 26, 2020

Copyright © 2020 by author(s) and Open Access Library Inc.

This work is licensed under the Creative Commons Attribution International License (CC BY 4.0).

<http://creativecommons.org/licenses/by/4.0/>



Open Access

Abstract

In order to improve the reliability of busbar protection, a new fast busbar protection algorithm based on active power and extreme learning machine is proposed. By performing S-transformation on the fault voltage and current traveling wave, the active power amplitude within 0.1 ms after the fault is obtained. Simulate different fault types in the busbar area and build a bus fault feature vector sample set. The intelligent model of fault learning of extreme learning machine is established, and the sample set is used for training and testing to realize bus fault area identification. The simulation results show that the proposed busbar protection method can identify faults in the busbar area sensitively and reliably.

Subject Areas

Analytical Chemistry, Applied Physics, Complex Network Models, Mathematical Analysis, Mathematical Economics

Keywords

Busbar Protection, Extreme Learning Machine, Active Power, S Transform, Fault Identification

1. Introduction

Busbar protection plays an important role in the power system and bears the responsibility of transmitting electrical energy [1] [2]. When a fault occurs on the bus, if it cannot be processed in time, it will inevitably affect the stable operation of the power system and even cause the regional power system to collapse [3]. In order to prevent the serious consequences of the busbar fault, special busbar protection should be set to timely and correctly interrupt the faulty busbar short-circuit current. The protection device should operate quickly and reliably

to shorten the fault removal time and ensure the stable operation of the power grid [4] [5]. In order to prevent the serious consequences of busbar faults, special busbar protection should be set to timely and correctly interrupt all busbar short-circuit currents, which puts higher requirements on the performance of busbar protection.

The protection of power frequency in busbar protection is the most widely used in current differential protection, but it may be misjudged due to problems such as TA error and TA saturation [6], and the action speed is slow, and it is protected in the super/extra high voltage grid. Performance does not meet system operating requirements. Although transient protection can achieve rapid protection, there is still a small initial angle [7]. The literature [8] defines the transient traveling wave power. The wavelet transform method is used to identify and compare the transient traveling wave power polarity of each line. According to the polarity characteristics of the traveling wave power of all lines in the fault, the busbar area is discriminated. External failure, but did not solve the effect of small initial angle of failure. In [9], the directional traveling wave on each outgoing line in a specific time period after the fault is integrated, and the busbar fault is established by analyzing the magnitude of the forward and backward traveling wave integral ratio.

In recent years, S-transformation and power theory have been more maturely used in power systems [10] [11] [12]. In [10], the fault direction identification is realized by using the S-transformed power difference between the active power and the busbar. Reference [11] uses the S-transform reactive power to detect the fault direction when the amplitude of the reactive power is outside the busbar.

This paper draws on the direction traveling wave and power theory described in the literature [10] [11] [12], combined with the application of S transform in power system [13] [14] [15], calculates the voltage and current traveling wave S transform active for a period of time after each fault of the busbar line. Power is combined with the limit learning machine to achieve faults inside and outside the busbar.

2. Fault Current Traveling Wave Characteristics Analysis

2.1. The Basic Theory of Fault Traveling Waves

Figure 1 shows the busbar of the 500 kV substation, L1 - L4 are the four lines connected by the busbar M, and R1 - R4 are the traveling wave protection units installed at the M end of the corresponding bus near the bus. When the fault occurs at the F2 on the line L2, The wave propagates from the fault point along the line to both sides and deflection occurs at the discontinuity of the wave impedance. For any point on the line from the fault point x , the transient voltage and current at this point are obtained [9]:

$$\begin{cases} \Delta u(x, t) = \Delta u_+(x - tv) + \Delta u_-(x + tv) \\ \Delta i(x, t) = \Delta i_+(x - tv) + \Delta i_-(x + tv) \\ v = 1/\sqrt{LC} \end{cases} \quad (1)$$

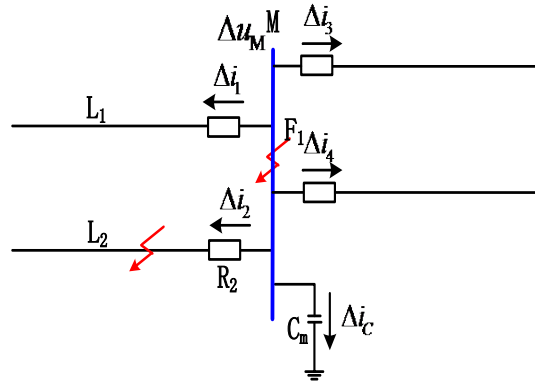


Figure 1. Sketch map of 500 kV busbar system.

where: t is the observation time, L and C are the inductance and capacitance of the line per unit length; Δu_+ (Δu_-), Δi_+ (Δi_-) are the forward (reverse) traveling waves of voltage and current propagating along the positive (reverse) direction of X .

According to the traveling wave propagation theory, the time when the initial traveling wave reaches the bus bar M is t_0 , the traveling wave is deflected and reflected for the second time to reach the bus bar. The moment is t_1 , so in $t_0 \sim t_1$ time period, the fault traveling wave obtained by the protection unit R_k ($k = 1, 2, 3, 4, 5$) of each associated line of the bus bar is called an initial voltage and a current traveling wave. among them, the Δu_M is initial voltage traveling wave for bus M. Δi_k ($k = 1, 2, 3, 4$) is the current traveling wave measured for each line of the bus. $Z_{c1} \sim Z_{c4}$ are the wave impedances of the associated lines L1 to L5 of the bus bar, and the equivalent impedance of the bus line M to the ground stray capacitance is Z_{cm} .

2.2. Analysis of Fault Current Traveling Wave Propagation Process

2.2.1. Characteristics of Current Traveling Wave in Busbar Internal Fault

The analysis shows that the transient voltage and current at any point on the line are superposition of the forward and reverse traveling waves. The current forward and reverse traveling waves obtained by Equation (1) are [9]:

$$\begin{cases} \Delta i_+ = \frac{1}{2} \left[\Delta i + \frac{\Delta u}{z_c} \right] \\ \Delta i_- = \frac{1}{2} \left[\Delta i - \frac{\Delta u}{z_c} \right] \end{cases} \quad (2)$$

Δu , Δi are the voltage and current fault components measured for each line R, and Z_c is the line wave impedance.

It can be seen from the propagation characteristics of the traveling wave that the traveling wave at the fault point and the bus bar will be deflected [9]. Referring to **Figure 1**, the positive direction of the traveling wave is defined as the bus line pointing to the line. When the internal fault of the bus line occurs, the

traveling mode of the traveling wave is as shown in **Figure 2**, among them, Δi_{n+} ($n = 1, 2, 3, 4, 5$) is the forward traveling wave of the n th associated line.

When an internal fault occurs in the busbar, each outgoing line is a transmission line with evenly distributed parameter characteristics, and the wave impedance does not deflect on the line. Let the length of the shortest line L among the associated lines be d_{\min} . Only the initial forward traveling wave is detected at each associated line R in the $[t_0, t_0 + 2d_{\min}/v]$ time period, and there is no reverse traveling wave formed by the forward traveling wave reflection.

2.2.2. Initial Traveling Wave Power Distribution in Case of Internal Fault of Bus M

The Peterson equivalent circuit of bus m in case of point F_1 fault is shown in **Figure 3**, where $\Delta \dot{u}_m$ is the traveling wave vector of the initial voltage of bus M measured, and $\Delta \dot{I}_k$ ($k = 1, 2, 3, 4, 5$) is the traveling wave vector of the current measured by the M terminal protection unit of each line connected to the bus. The wave impedances of lines $L_1 \sim L_5$ are $Z_{c1} \sim Z_{c5}$ and Z_{cm} are equivalent impedances of stray capacitance of bus m to ground.

When S transforms, the traveling wave frequency is $f = 50 \sim 100$ kHz, when the super (extra) high-voltage transmission line wave impedance can be approximated as a real constant, it is equivalent to the resistance [15] in the Peterson equivalent circuit, and the bus-to-ground equivalent capacitance impedance $Z_{cm} = 1/j\omega C_m = 1/j2\pi f C_m$ is imaginary (f is corresponding traveling frequency).

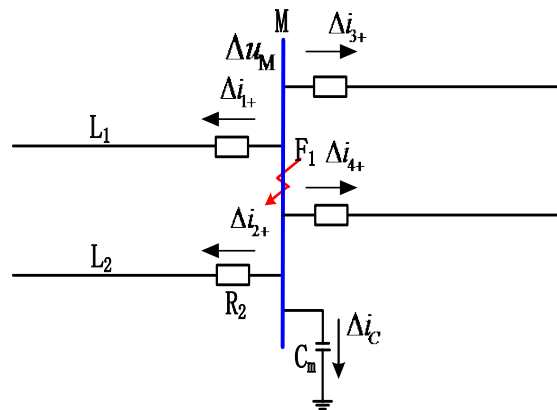


Figure 2. Propagation of fault traveling wave in fault of bus.

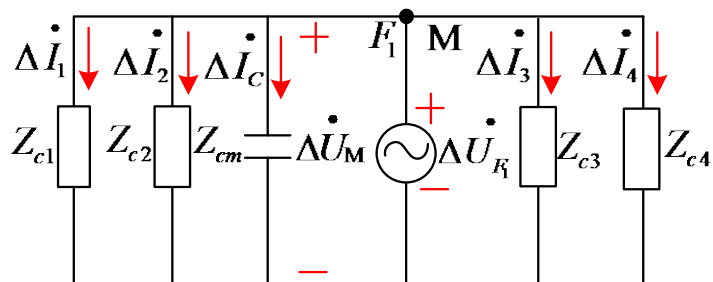


Figure 3. Equivalent circuit based on Peterson principle for busbar internal fault.

From the definition of the initial traveling wave complex power [15], taking the L1 line as an example, the initial traveling wave complex power of the M-side of the near-busbar of the line can be obtained as:

$$\Delta S_1 = \Delta u_M \Delta i_1^* \tag{3}$$

when the internal F1 point of the busbar fails, the Peterson equivalent circuit of **Figure 3** shows:

$$\Delta i_1 = \Delta u_M (1/Z_{c1}) \tag{4}$$

Since the line wave impedance is approximately a real constant, it is equivalent to the resistance [16]-[19] in the equivalent circuit, and the complex power measured by the M1 IED1 protection unit of the L1 line can be obtained:

$$\begin{aligned} \Delta \tilde{S}_1 &= \Delta \dot{U}_M \Delta \dot{i}_1^* = \Delta \dot{U}_M \times [\Delta \dot{U}_M^* (1/Z_{c1})] \\ &= \Delta U_M^2 \times (1/Z_{c1}) = P_1 + jQ_1 \end{aligned} \tag{5}$$

In the middle: P_1 is the initial traveling wave active power of the line, and Q_1 is the initial traveling wave reactive power of the line, when the busbar internal fault occurs:

$$P_1 = \Delta U_M^2 \times (1/Z_{c1}) \tag{6}$$

Similarly, the initial traveling wave active power measured by the M-side protection unit of other lines connected to the busbar can be derived:

$$P_i = \Delta U_M^2 / Z_{ci} \quad (i = 1, 2, 3, 4, 5).$$

Ideally, due to the internal fault of the bus, the wave impedance $Z_i (i = 1, 2, 3, 4)$ of each line is almost the same. According to formula (5), the initial traveling wave active power measured by all associated lines of the bus is basically the same, that is $P_1 \approx P_2 \approx P_3 \approx P_4$, is greater than 0.

2.2.3. Current Traveling Wave Characteristics of Busbar External Fault

Figure 4 shows the propagation of forward and reverse traveling waves when line L2 fails. Among them, Δi_{n+} ($n = 1, 2, 3, 4$) is the forward traveling wave of each associated line, Δi_{2-} is the reverse traveling wave of the line L2, since the reverse traveling wave of the line L2 forms a buckling reflection when reaching

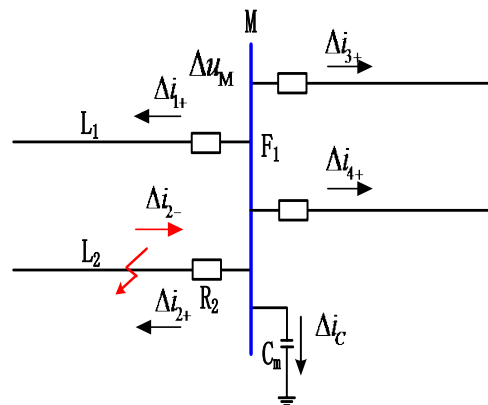


Figure 4. Propagation of fault traveling wave in fault of bus.

the bus bar, forming a forward wave Δi_{2+} formed by the reflection of the reverse traveling wave. Only the faulty line detects the reverse traveling wave during the $[t_0, t_0 + 2d_{dim}/v]$ time period.

In summary, when the bus line fails, the associated lines are in the $[t_0, t_0 + 2d_{dim}/v]$ time period, only the forward traveling wave is detected; when the bus area outside the fault occurs, when an out-of-bus fault occurs within the time period $[t_0, t_0 + 2d_{dim}/v]$, the reverse traveling wave can only be detected on the faulty line.

2.2.4. Initial Traveling Wave Power Distribution When Bus M External Fault

When the F2 point on the L2 line fails, the Peterson equivalent circuit of the bus M is as shown in **Figure 5**.

As can be seen from **Figure 5**:

$$\Delta \dot{I}_2 = -\Delta \dot{U}_M (1/Z_{c1} + 1/Z_{c3} + 1/Z_{c4} + j\omega C_m) \tag{7}$$

The complex power measured by the L2 fault line near the bus M-side protection unit IED2 can be obtained:

$$\begin{aligned} \Delta \tilde{S}_2 &= \Delta \dot{U}_M \Delta \dot{I}_2^* \\ &= \Delta \dot{U}_M \times \left[-\Delta \dot{U}_M^* (1/Z_{c1} + 1/Z_{c3} + 1/Z_{c4} - j\omega C_m) \right] \\ &= -\Delta U_M^2 \times (1/Z_{c1} + 1/Z_{c3} + 1/Z_{c4}) + \Delta U_M^2 \times j\omega C_m \\ &= P_2 + jQ_2 \end{aligned} \tag{8}$$

That is, when the busbar external fault occurs, the initial traveling wave active power of the faulty line is:

$$P_2 = -\Delta U_M^2 \times (1/Z_{c1} + 1/Z_{c3} + 1/Z_{c4}) \tag{9}$$

For the non-faulty line connected to bus M, take L3 as an example. In **Figure 5**:

$$\Delta \dot{I}_3 = \Delta \dot{U}_M (1/Z_{c3}) \tag{10}$$

The complex power measured by the M-side IED3 protection unit of the L3 line:

$$\begin{aligned} \Delta \tilde{S}_3 &= \Delta \dot{U}_M \Delta \dot{I}_3^* = \Delta \dot{U}_M \times \left[\Delta \dot{U}_M^* (1/Z_{c3}) \right] \\ &= \Delta U_M^2 \times (1/Z_{c3}) = P_3 + jQ_3 \end{aligned} \tag{11}$$

$$P_3 = \Delta U_M^2 / Z_{c3} \tag{12}$$

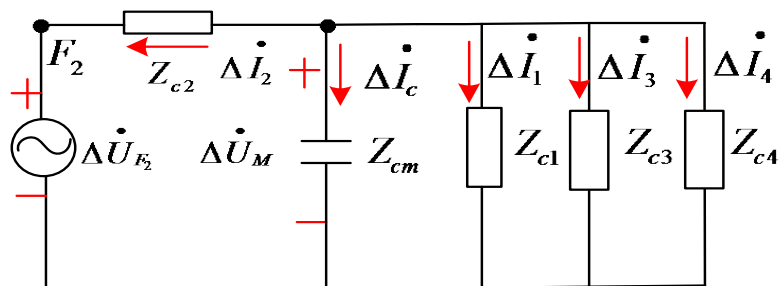


Figure 5. Equivalent circuit based on Peterson principle for busbar external fault.

Similarly, the initial traveling wave active power measured by the M-side protection unit of other non-faulty lines connected to the busbar can be obtained: $P_i = \Delta U_M^2 / Z_{ci} (i = 1, 4)$.

3. Calculate the Initial Traveling Wave Active Power Based on the S Transform

3.1. Basic Principle of S Transform

S transform is a reversible local time-frequency analysis method, which avoids the selection of window function and improves the fixed window width defects. At the same time, the feature quantity extracted by S transform is not sensitive to noise [17].

Set the continuous time signal to $h(t)$, then the continuous S transform of the time signal is defined as:

$$\begin{cases} S(\tau, f) = \int_{-\infty}^{\infty} h(t) g(\tau - t, f) e^{-i2\pi ft} dt \\ g(\tau - t, f) = \frac{|f|}{\sqrt{2\pi}} e^{-\frac{(\tau-t)^2}{2\sigma^2}} \end{cases} \quad (13)$$

τ is the parameter that controls the position of the Gaussian window on the time axis, f is the continuous frequency, t is the time, i is the imaginary number, $\sigma = 1/|f|$, $g(\tau - t, f)$ is a Gaussian window and is affected by frequency changes.

If $h[kT] (k = 0, 1, 2, \dots, N-1)$ is the signal $h(t)$ discrete time series obtained by sampling, T is the sampling interval and N is the number of sampling points. The discrete Fourier transform function of $h[kT]$ is:

$$h\left[\frac{n}{NT}\right] = \frac{1}{N} \sum_{k=0}^{N-1} h[kT] e^{-j\frac{2\pi kn}{N}} \quad (14)$$

where $n = 0, 1, \dots, N-1$

The discrete S transform of signal $h(t)$ is:

$$\begin{cases} S\left[kT, \frac{n}{NT}\right] = \sum_{r=0}^{N-1} H\left(\frac{r+n}{NT}\right) e^{-\frac{2\pi^2 r^2}{n^2}} e^{j\frac{2\pi rk}{N}}, n \neq 0 \\ S[kT, 0] = \frac{1}{N} \sum_{r=0}^{N-1} h\left(\frac{r}{NT}\right), n = 0 \end{cases} \quad (15)$$

A complex time-frequency matrix is obtained by S transform, which reflects the time domain and frequency domain characteristics of the signal and the amplitude information of the traveling wave in the time domain.

3.2. Calculation of Initial Traveling Wave Active Power

For a three-phase transmission system, there is a coupling between each phase voltage and each phase current, which is generally decoupled by phase-mode transformation. In this paper, the combined modulus method is used to transform the phase mode to reflect various fault types [17]:

$$\Delta i_z = 4\Delta i_\alpha + \Delta i_\beta \quad (16)$$

$$\Delta u_z = 4\Delta u_\alpha + \Delta u_\beta \quad (17)$$

Among them, $\Delta u_\alpha, \Delta i_\alpha$ are the voltage and current traveling wave α line mode components after decoupling treatment, Δu_β and Δi_β are the processed voltage and current traveling wave β line mode components.

In this paper, the method used in [18] [19] is used to perform discrete S-transformation on the transformed combined modulus fault voltage and current traveling wave modulus, and extract the phasor corresponding to 20 sampling points of the single-frequency initial traveling wave.

The combined modulus current Δi_2 obtained by the IED2 protection unit after a three-phase short circuit occurs at point F2 on line L2 as an example, discrete S-transform principle Δi_2 according to the above-mentioned S-transform principle, and one-dimensional complex vector [18] [19] is obtained on selected frequency f_z , which can be expressed as:

$$\Delta l_{2n}(t_n, f_z) = \Delta l_{2n}(t_n, f_z) \exp[j\theta_{2n}(t_n, f_z)] \quad (18)$$

$\Delta l_{2gn}(t_n, f_z), \theta_{2gn}(t_n, f_z)$ are the amplitude of $\Delta l_{2gn}(t_n, f_z)$, where n is the sampling point n and t_n is the sampling time of the sampling point n .

After the fault occurs, the transient traveling wave reaches the bus M after a period of time and propagates on the bus associated line. The L2 line near-bus M-side protection unit IED2 captures the initial traveling wave, if the amplitude of the line is Δl_{21} at the moment of t_1 , $\Delta l_{2g1}(t_1, f_z)$ obtained at the selected frequency f_z is the corresponding initial current traveling wave phasor at that time [18] [19]. Similarly, the initial voltage traveling wave phasor $\Delta U_{M1}(t_1, f_z)$ measured by bus M at time t_1 can be obtained. The other non-faulty line associated with the bus is near the bus end at the selected frequency f_z . The phasors corresponding to the 20 initial sampling points of the initial current traveling wave are $\Delta l_{1n}(t_n, f_z), \Delta l_{3n}(t_n, f_z)$ and $\Delta l_{4n}(t_n, f_z) (n=1, 2, \dots, 20)$.

Under the selected S-transform single frequency, using the phasor corresponding to each sampling point of the initial traveling wave obtained by the above-mentioned derivation, the active power corresponding to 20 sampling points of the initial traveling wave of each associated line in the occurrence of the out-of-area fault of the bus M can be calculated.

Based on the above analysis, when the busbar is internally generated, the initial traveling wave active power measured by each associated line of the busbar is $\Delta U_{M \cdot n}^2(t_n, f_z)/Z_{ci}$, where $i=1, 2, 3, 4$; When the busbar is external, the initial traveling wave active power measured by the faulty line is $\Delta U_{M \cdot n}^2(t_n, f_z)/(1/Z_{c1} + 1/Z_{c3} + 1/Z_{c4})$ (assuming L2 line fault as an example), non-fault line active power is $\Delta U_{Mgn}(t_n, f_z)/Z_{ci} (i=1, 3, 4)$.

4. Extreme Learning Machine

The feedforward neural network is a kind of artificial neural network [20]. In this neural network, each neuron starts from the input layer, receives the input of the previous stage, and inputs it to the next stage until the output layer. There

is no feedback throughout the network, and a directed acyclic graph can be used. The feedforward neural network is the earliest proposed artificial neural network and the simplest type of artificial neural network. According to the number of layers of the feedforward neural network, it can be divided into a single layer feedforward neural network and a multilayer feedforward neural network. Among them, common feedforward neural networks include BP neural network [20], radial basis function (RBF) neural network [20] and extreme learning machine (ELM) neural network [20].

Extreme learning machine is an easy-to-use and effective single-hidden layer feedforward neural network SLFN learning algorithm [20]. The network consists of input layer, hidden layer and output layer, input layer and hidden layer and hidden layer. Among them, the input layer has n neurons, corresponding to n input variables; the hidden layer has 1 neuron; the output layer has m neurons, corresponding to m output variables. **Figure 6** is a block diagram of a single hidden layer ELM network.

ELM only needs to set the number of hidden layer neurons in the network. It does not need to adjust the input weight of the network and the bias of the hidden element during the execution of the algorithm. Compared with the traditional neural network [21] [22], it changes. The BP neural network is based on the gradient descent learning idea. It does not need to iteratively update the network parameters. It changes the SVM learning performance and relies on the parameter adjustment. It has the advantages of fast learning speed and good generalization performance, and only produces the unique optimal solution.

Given N different training samples (x_i, t_i) , among them,

$$\begin{aligned} x_i &= [x_{i1}, x_{i2}, \dots, x_{im}]^T \in R^n \\ t_i &= [t_{i1}, t_{i2}, \dots, t_{im}]^T \in R^m \end{aligned} \quad (19)$$

Given an excitation function $g(x)$, after that, the output containing L hidden layer nodes can be expressed as,

$$\sum_{i=1}^L \beta_i g(a_i x_j + b_i) = \sum_{i=1}^L \beta_i G(a_i, b_i, x_j) = t_i \quad (20)$$

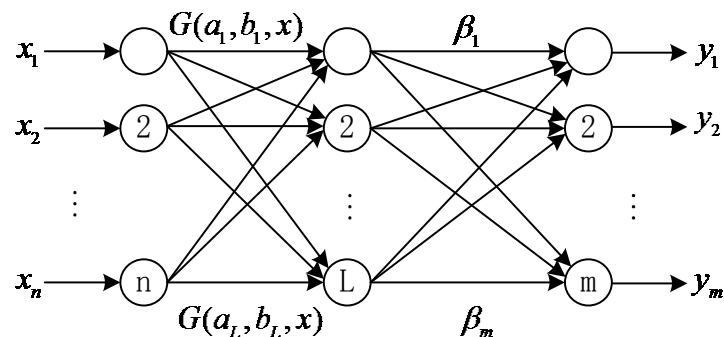


Figure 6. ELM network structure.

Among them, $j=1,2,\dots,N$; $a_i = [a_{i1}, a_{i2}, \dots, a_{in}]^T$ is the input weight of the input node and the i -th hidden layer node; b_i is the neuron offset for the i -th hidden layer node; $\beta_i = [\beta_{i1}, \beta_{i2}, \dots, \beta_{im}]^T$ is the output weight of the i -th hidden layer node and the output node.

The algorithm steps are as follows:

1) Randomly selected (a_i, b_i) and map sample to the new feature space through $h(x) = [G(a_1, b_1, x), \dots, G(a_L, b_L, x)]^T$. If the hidden layer matrix H is formed by the random feature map $h(x)$, then:

$$H\beta = T \quad (21)$$

Among it,

$$H = \begin{bmatrix} h(x_1) \\ \vdots \\ h(x_N) \end{bmatrix} = \begin{bmatrix} G(a_1, b_1, x_1) & \cdots & G(a_L, b_L, x_1) \\ \vdots & \ddots & \vdots \\ G(a_1, b_1, x_N) & \cdots & G(a_L, b_L, x_N) \end{bmatrix},$$

$$\beta = \begin{bmatrix} \beta_1^T \\ \vdots \\ \beta_L^T \end{bmatrix}_{L \times m} \quad \text{and} \quad T = \begin{bmatrix} t_1^T \\ \vdots \\ t_N^T \end{bmatrix}_{N \times m}$$

Sigmoid function is selected as the excitation function of hidden layer node

$$g(a_i x_j + b_i) = \frac{1}{1 + \exp(-a_i x_j + b_i)}$$

2) In the new feature space, the optimal output weight $\hat{\beta}$ and $\hat{\beta} = H^+ T$ are sought by least squares method by Equation (12), where H^+ is the Moore Penrose generalized inverse of H .

5. Bus Fault Area Identification Method

T-line line traveling wave protection R_k ($k=1,2,3,4$) unit after fault detected voltage and current traveling wave is S-transformed and the S-transform single frequency is selected to be 60 kHz. Select different transition resistances, different fault types and different initial angles of the fault to simulate the faults of the bus and the associated line. The out-of-area lines are simulated according to the same fault and different fault distances are set as simulation conditions. Bus internal fault and external fault constitute active power vector ∇P , among them:

$$\nabla P_m = [\nabla P_{m1} \nabla P_{m2} \cdots \nabla P_{m5}]_{1 \times 5}$$

And $\nabla P_{mi} = [P_1 P_2 \cdots P_{20}]_{1 \times 20}$ ($m=1,2,3,4; i=1,2,3,4$), ∇P indicates bus fault data, The initial traveling wave active power vector of the fault in the busbar is combined into a bus fault characteristic vector ∇P . In this way, the bus fault feature is characterized, and the fault region label is used as the sample data of the extreme learning machine, wherein

$$\nabla P = [\nabla P_{11} \cdots \nabla \hat{P}_{M1} \nabla P_{21} \cdots \nabla \hat{P}_{M2} \nabla P_{31} \cdots \nabla \hat{P}_{M3}]_{1 \times 15}$$

The fault identification algorithm flow is shown in **Figure 7**.

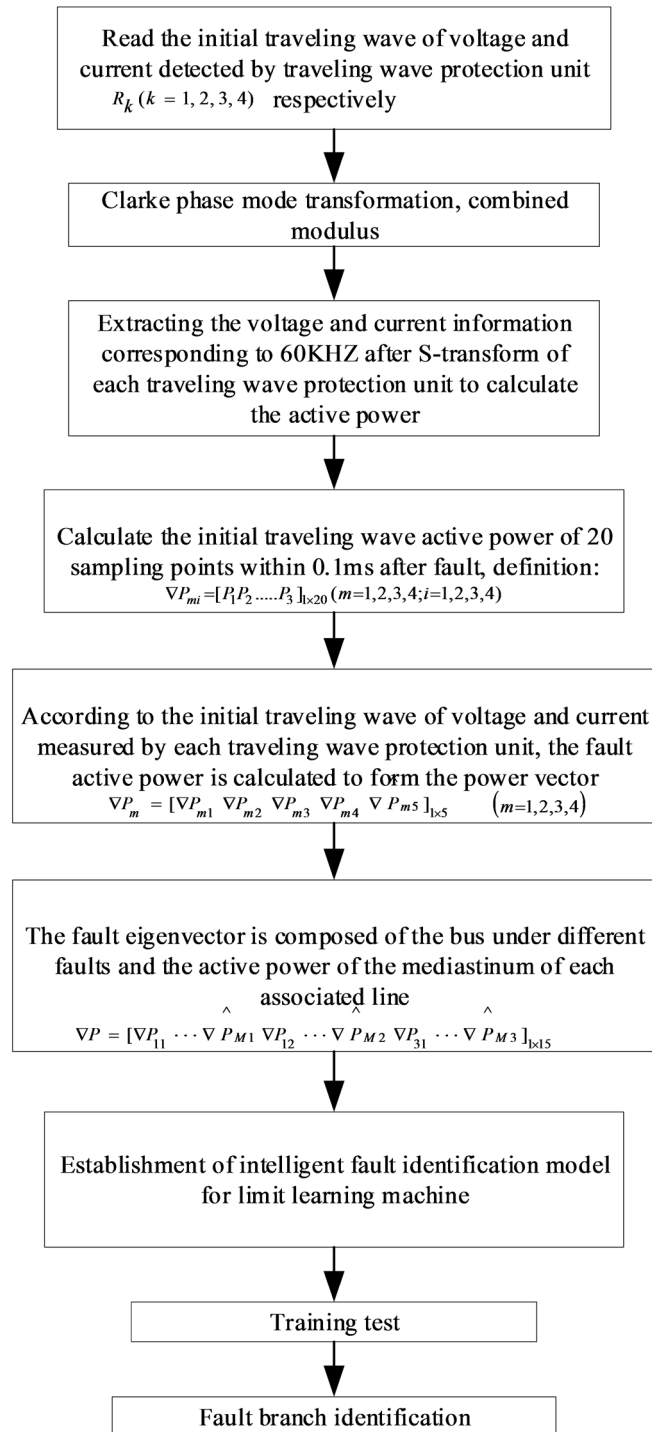


Figure 7. Flow chart of fault branch identification algorithm.

6. Simulation and Experiment

The PSCAD/EMTDC electromagnetic transient simulation software is used to establish the 500 kV T connection line simulation model shown in **Figure 1**. The line model uses a frequency-dependent distributed parameter model that can accurately reflect transient and harmonic responses. The line type uses TOWER:

3H5 tower. The simulation sampling frequency is 200 kHz, and the lengths of each branch are $L_1 = 230$ km, $L_2 = 250$ km, $L_3 = 300$ km, and $L_4 = 210$ km. Select the S-transform single frequency to calculate the fault active power under different conditions of different transition resistances, different fault types and different initial angles of the fault, and form the active power vector

$\nabla P_m = [\nabla P_{m1} \nabla P_{m2} \dots \nabla \hat{P}_{m5}]_{1 \times 5}$. Combine active power under different transition

resistances, different fault types and different initial angles of faults into fault eigenvectors ∇P . In order to characterize the fault characteristics in the busbar area, the sample set required by the extreme learning machine is established accordingly, wherein $\nabla P = [\nabla P_{11} \dots \nabla \hat{P}_{M1} \nabla P_{21} \dots \nabla \hat{P}_{M2} \nabla P_{31} \dots \nabla P_{M3}]_{1 \times 15}$.

6.1. Sample Data

In order to verify the effectiveness and reliability of the algorithm, this paper chooses to carry out simulation experiments in the busbar area and outside under different fault types, different transition resistances, and different initial angles of faults.

The training samples of the extreme learning machine are composed of the active power of each line in the associated line of the busbar and the internal fault of the busbar. The random fault samples of the bus-line associated line are 96 fault eigenvectors obtained by simulating three different faults for the four branches outside the zone under different fault conditions. At the same time, in order to improve the reliability of the algorithm, different fault distances are set in the fault.

6.2. Extreme Learning Machine Intelligent Fault Recognition Model Establishment and Training Sample Test Analysis

The fault characteristic training sample is input into the limit learning machine for training, and a trained extreme learning machine bus fault recognition model is obtained. Among them, the optimal number of neurons in the hidden layer of the extreme learning machine obtained by the trial and error method is 35.

The fault characteristic training samples are input into the trained extreme learning machine intelligent fault recognition model for testing, and the comparison of the predicted results is shown in **Figure 8**.

It can be seen from the above figure that the test sample data in the extreme learning machine fault intelligent recognition model has a correct rate of 100%.

6.3. Test Sample Test Analysis

6.3.1. Different Fault Initial Angle Test

The fault characteristic test samples of different initial angles of the faults are input into the intelligent learning model of the limit learning machine busbar fault area for testing. The comparison of the prediction results is shown in **Figure 9**, wherein **Table 1** is the simulation verification result corresponding to the fault condition.

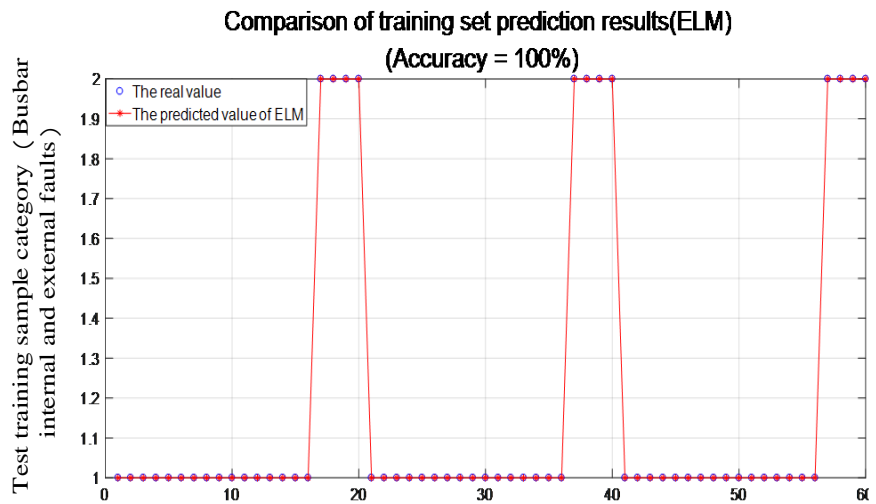


Figure 8. Comparison of training set prediction results.

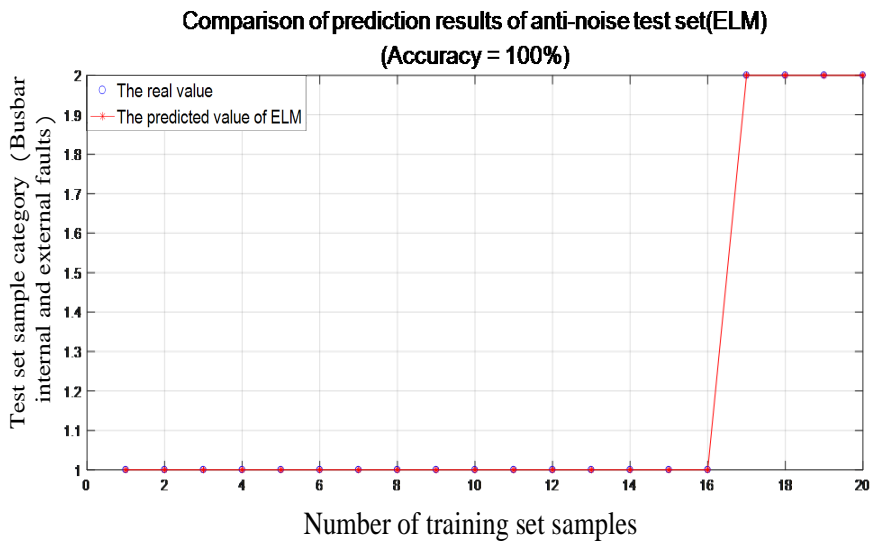


Figure 9. Comparison of test set prediction results.

Table 1. Test results of protection algorithm under different inception angles for external fault of bus.

Fault location	Transition resistance Ω	Fault initial angle	Fault distance	fault type	Decision result
Line, L1, L2, L3, L4	100	5	Distance from bus M 80 km	Phase B short circuit to ground	External
		45			External
		90			External
		100			External
Busbar M	300	5		Phase B short circuit to ground	Internal
		45			Internal
		90			Internal
		100			Internal

It can be seen from the above chart that the accuracy of the test results in the extreme learning machine fault intelligent identification model is 100%, and the faults in the zone can be identified when different types of faults occur in the busbar area, so the protection algorithm is not affected by the initial angle of the fault.

6.3.2. Analysis of Different Transition Resistance Tests

The fault characteristic test samples of different transition resistances in the area and outside are input into the intelligent learning model of the limit learning machine busbar fault area for testing. The comparison of the prediction results is shown in Figure 10 and Table 2 is the simulation verification result corresponding to the fault condition.

It can be seen from the above chart that the test sample data in the extreme learning machine intelligent fault identification model test results in a correct rate of 100%, in the occurrence of different transition resistance faults within the busbar area and outside can accurately identify the faults inside and outside the area, so the fault identification algorithm is not The effect of the transition resistance.

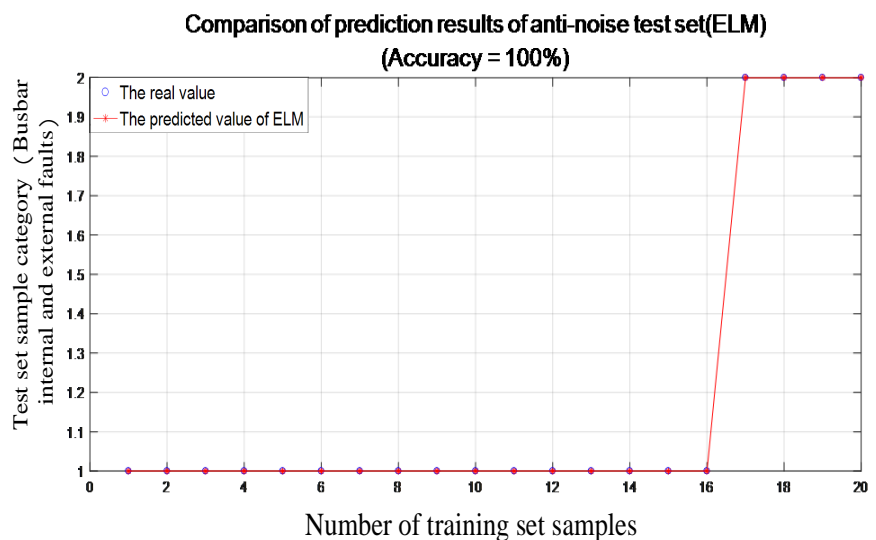


Figure 10. Comparison of training set prediction results.

Table 2. Test results of protection algorithm under different transition resistance in case of external fault of bus.

Fault location	Transition resistance Ω	Fault initial angle/($^{\circ}$)	Fault distance	fault type	Decision result
Line, L1, L2, L3, L4	0	45 $^{\circ}$	Distance from bus M 100 km	BC phase short to ground	External
	200				External
	500				External
	800				External
Bus M	0	45 $^{\circ}$		Phase an earth fault	Internal
	200				Internal
	500				Internal
	800				Internal

6.3.3. Testing of Different Fault Types

The fault characteristic test samples tested by different fault types in the area and outside are input into the intelligent learning model of the limit learning machine bus fault area for testing. The comparison of the predicted results is shown in **Figure 11**, wherein **Table 3** is the simulation verification result corresponding to the fault condition.

It can be seen from the above chart that the test sample data has a correct rate of 100% in the test of the intelligent learning model of the extreme learning machine, and can accurately identify the faults in the area and outside under different fault types, so the protection algorithm is basically not affected by the fault type.

Based on the above analysis, the proposed algorithm is not affected by the initial angle of the fault, the transition resistance and the type of fault, and can reliably identify the fault area.

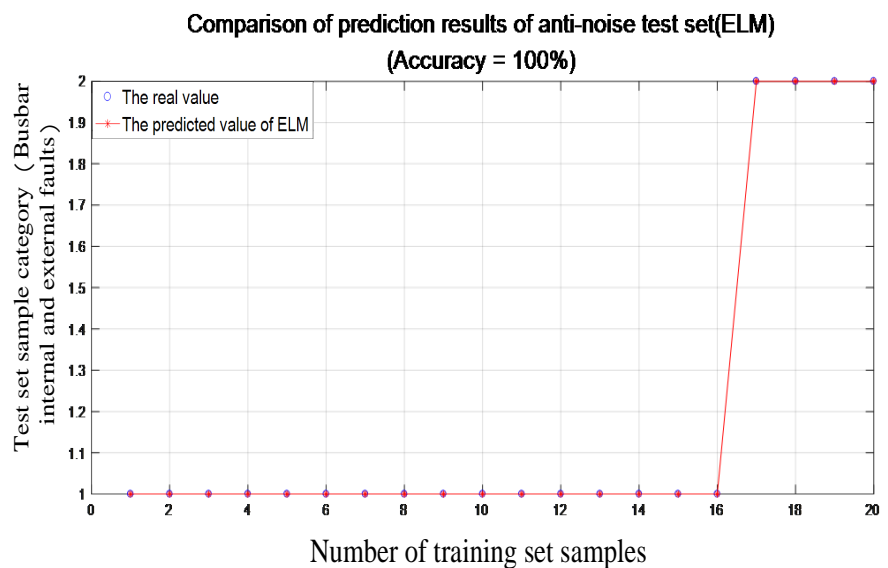


Figure 11. Comparison of training set prediction results.

Table 3. Test results of protection algorithm under different fault types in case of external fault of bus.

Fault location	Transition resistance/(°)	Fault initial angle	Fault distance	Transition resistance Ω	Decision result
Line, L1, L2, L3, L4	AG	45°	Distance from bus M 20 km	80	External
	ABG				External
	BC				External
	ABC				External
Bus M	AG	45°		200	Internal
	ABG				Internal
	BC				Internal
	ABC				Internal

7. Conclusions

This paper proposes a new fast bus protection algorithm based on the combination of active power and extreme learning machine. By performing S-transformation on the fault voltage and current traveling wave, the active power amplitude within 0.1 ms after the fault is utilized. The feasibility of the fault identification method is verified by a large number of simulation experiments. The theoretical and simulation results show that:

- 1) The algorithm identifies the fault area by establishing the intelligent identification model of the bus fault area. In the simulation analysis under various working conditions, the fault can quickly and accurately identify the fault area, which basically overcomes the influence of transition resistance and initial angle of fault.
- 2) The protection algorithm only uses the information of the initial traveling wave of the voltage and current, the criterion is simple, the setting is easy, the required data window is short, and the communication volume is small.
- 3) Compared with the traditional bus fault region identification algorithm, the algorithm shows better performance in motion speed and fault identification accuracy.

Acknowledgements

This research was supported by Project Supported by Sichuan Science and Technology Department Project (2017JY0338, 2019YJ0477, 2018GZDZX0043, 2018JY0386); Artificial Intelligence Key Laboratory of Sichuan Province (2019RYY01); Enterprise Informatization and Internet of Things Measurement and Control Technology Sichuan University Key Laboratory Project (2018WZY01); Sichuan Institute of Science and Technology Sichuan Academician (Expert) Workstation Project (2018YSGZZ04); Science and Technology Project Funding of State Grid Corporation of China (Contract No.521997180016).

Conflicts of Interest

The authors declare no conflicts of interest regarding the publication of this paper.

References

- [1] Solovev, D.B. and Kuzora, S.S. (2016) Implementation of Noise-Immune Rogowski Coils for Busbar Differential Protection Modernization. *Electric Power Systems Research*, **140**, 965-966. <https://doi.org/10.1016/j.epsr.2016.03.039>
- [2] Suonan, J.L., Deng, X.Y., Jiao, Z.B., *et al.* (2010) A Novel Principle of Integrated Impedance Based Bus-Bar Protection. *Power System Protection and Control*, **38**, 1-7.
- [3] Guo, Z.W., Yao, J.G. and Tan, Z.W. (2015) Hilbert-Huang Transform-Based Transient Busbar Protection Algorithm. *IET Generation, Transmission & Distribution*, **9**, 2032-2039. <https://doi.org/10.1049/iet-gtd.2014.0719>

- [4] Song, F.F., Wang, Z.P. and Liu, Y. (2003) Status Quo and Development Tendency of Busbar Protection. *Electric Power Automation Equipment*, **23**, 66-69.
- [5] Gil, M. and Abdoos, A.A. (2017) Intelligent Busbar Protection Scheme Based on Combination of Support Vector Machine and S-Transform. *IET Generation, Transmission & Distribution*, **11**, 2056-2064.
<https://doi.org/10.1049/iet-gtd.2016.1686>
- [6] Zou, G.B. and Gao, H.L. (2013) Fast Pilot Protection Method Based on Waveform Integral of Traveling Wave. *International Journal of Electrical Power & Energy Systems*, No. 50, 1-8. <https://doi.org/10.1016/j.ijepes.2013.02.009>
- [7] Huang, R.C., Yan, H.Y. and Cui, D.S. (2003) Busbar Protection Based on Current Traveling Waves. *Relay*, **31**, 26-28.
- [8] Duan, J.D., Zhang, B.H. and Zhang, S.X. (2004) A Distributed Bus Protection Using Transient Traveling Wave Power Directions of Transmission Lines. *Proceedings of the CSEE*, **24**, 7-12.
- [9] Zou, G.B., Song, S.L., Xu, C.H., *et al.* (2014) Fast Busbar Protection Based on Waveform Integral of Directional Traveling Waves. *Proceedings of the CSEE*, **34**, 5677-5683.
- [10] Wu, H., Dong, X.X. and Wang, Q.M. (2019) A New Principle for Initial Traveling Wave Active Power Differential Busbar Protection. *IEEE Access*, **7**, 70495-70512.
<https://doi.org/10.1109/ACCESS.2019.2917044>
- [11] Wu, H., Dong, X.X. and Ye, R.K. (2019) A New Algorithm for Busbar Protection Based on the Comparison of Initial Traveling Wave Power. *IEEE Transactions on Electrical and Electronic Engineering*, **14**, 520-533.
<https://doi.org/10.1002/tee.22835>
- [12] Wu, H., Li, Q.Z. and Liu, W. (2005) A New Pilot Protection Algorithm Based on Traveling Wave Power for Transmission Lines. *Automation of Electric Power Systems*, **29**, 51-54.
- [13] Wu, H. (2016) New Pilot Protection Principle Based on Fault Voltage Traveling Wave Energy Comparison for Transmission Lines. *High Voltage Apparatus*, **55**, 42-48.
- [14] Li, X.P., He, Z.Y., Wu, X., *et al.* (2014) Ultra High Speed Directional Element Based on Amplitude Comparison Using S-Transform Energy Relative Entropy. *Automation of Electric Power Systems*, **38**, 113-116.
- [15] Wu, H. (2016) A New Pilot Protection Principle Based on S-Transform Sample Entropy. *Power System Protection and Control*, **44**, 15-21.
- [16] Duan, J.D., Zhang, B.H., Ren, J.F., *et al.* (2007) Single-Ended Transient-Based Protection for EHV Transmission Lines Basic Theory. *Proceedings of the CSEE*, **27**, 37-43.
- [17] Chothani, N.G. and Bhalja, B.R. (2016) A New Algorithm for Busbar Fault Zone Identification Using Relevance Vector Machine. *Electric Power Components and Systems*, **44**, 193-205. <https://doi.org/10.1080/15325008.2015.1101725>
- [18] Duan, J.D., Zhang, B.H. and Chen, J. (2004) Study on the Current Traveling-Wave Differential Bus Protection. *Automation of Electric Power Systems*, **28**, 43-48.
- [19] Liu, X.M., Lin, S., He, Z.Y. and Liao, K. (2013) A Novel Surge Impedance Directional Relay Based on S Transform. *Proceedings of the CSEE*, **33**, 113-119.
- [20] Zhang, X.Q., Liang, J. and Zhang, X. (2013). Combined Model for Ultra Short-term Wind Power Prediction Based on Sample Entropy and Extreme Learning Machine. *Proceedings of the CSEE*, **33**, 33-40.

- [21] Huang, G.-B., Wang, D.H. and Lan, Y. (2011) Extreme Learning Machines: A Survey. *International Journal of Machine Learning and Cybernetics*, **2**, 107-122.
<https://doi.org/10.1007/s13042-011-0019-y>
- [22] Huang, G., Huang, G.-B., Song, S. and You, K. (2015) Trends in Extreme Learning Machines: A Review. *Neural Networks*, **61**, 32-48.
<https://doi.org/10.1016/j.neunet.2014.10.001>